Discriminating Uranium Isotopes Using the Time-Emission Profiles of Long-Lived Delayed Neutrons

J. Nattress, K. Ogren, A. Foster, A. Meddeb, Z. Ounaies, and I. Jovanovic

Phys. Rev. Applied **10**, 024049 — Published 30 August 2018

DOI: 10.1103/PhysRevApplied.10.024049

Discriminating Uranium Isotopes Using Long-lived Delayed Neutron Time Emission Profiles

J. Nattress,* K. Ogren, and I. Jovanovic†
Department of Nuclear Engineering and Radiological Sciences, University of Michigan, Ann Arbor, MI 48109 USA

A. Foster
Department of Materials Science and Engineering, Pennsylvania State University, University Park, PA 16802 USA

A. Meddeb and Z. Ounaies
Department of Mechanical and Nuclear Engineering, Pennsylvania State University, University Park, PA 16802 USA

In nuclear nonproliferation and safeguards, detecting and accurately characterizing special nuclear material remains one of the greatest challenges. Uranium enrichment determination is typically achieved by measuring the ratio of characteristic γ-ray emissions from ^{235}U and ^{238}U. Fission also produces β-delayed neutrons, which have been used in the past to determine uranium enrichment from the time dependence of the long-lived delayed neutron emission rate. Such measurements typically use moderated ^{3}He tube detectors. We demonstrate a new measurement technique that employs a fast neutron active interrogation probe and a scintillation detector to measure the enrichment of uranium using both the buildup and decay of β-delayed neutron emission. Instead of ^{3}He tubes, a capture-based heterogeneous composite detector consisting of scintillating Li-glass and polyvinyl toluene has been constructed and used, offering a prospect to scale delayed neutron measurements to larger detector sizes. Since the technique relies on the existing tabulated nuclear data, no calibration standards are required. It is shown that the buildup of delayed neutron emission can be used to distinguish between uranium samples and infer the uranium enrichment level, with accuracy that rivals the method that employs the time-dependent decay of delayed neutron emission.

I. INTRODUCTION

The ability to distinguish among different fissionable elements and isotopes is critical for many nuclear nonproliferation applications. For example, material accounting in fuel canisters located in enrichment facilities and verification of nuclear weapon dismantlement depend on measuring the isotopic fractions of ^{235}U and ^{238}U [1, 2]. Traditional nondestructive techniques for determining uranium enrichment rely on measuring the ratio of spontaneously emitted, characteristic γ rays from ^{235}U and ^{238}U [3–5]. Because of the energy-dependent attenuation of the γ-ray flux incident onto the detector due to shielding and self-shielding, prior knowledge or assumptions are needed for the geometry and characteristics of the sample and shielding. A less exploited method for measuring enrichment utilizes fission neutrons, which provide a unique time signature that is less sensitive to geometry and shielding. Further, neutrons experience much less attenuation in common γ-ray shielding materials [2].

Fission neutrons are produced in two time domains, prompt and delayed. The observation of delayed neutrons from fission is a well-established means for detecting fissionable materials [6–10]. Decay of fission products results in emission of delayed neutrons on a distinct, predictable characteristic decay timescale ranging from hundreds of milliseconds to tens of seconds. An important drawback of the delayed neutron signature is its low intensity, significantly below prompt neutron and γ-ray emission [11]. To establish the necessary signal time structure and increase the delayed neutron signal intensity, pulsed active interrogation (AI) sources are needed.

Characteristic β-delayed neutrons are commonly classified into several groups based on their respective precursors' lifetimes. These groups exhibit characteristic absolute yields and energy spectra, unique to the isotope and the inducing particle's type and energy. Methods used to date have exploited the short-lived delayed neutron groups to perform isotopic identification [7]. In other prior work, isotopic concentrations in pure uranium and mixed Pu-U samples were determined through the measurement of the decay of long-lived β-delayed neutron rate following irradiation [12–14]. When using a pulsed AI source, measurement of the delayed neutron time emission during irradiation is also possible, which we refer to as buildup, and provides complementary information regarding the interrogated material. To the best of our knowledge, however, measurement of the long-lived buildup of β-delayed neutron emission has not been used to determine the isotopic concentration of uranium or any other mixed fissile material sample. Further, no other detector types other than ^{3}He detectors have been

* jtnatt@umich.edu
† ijov@umich.edu

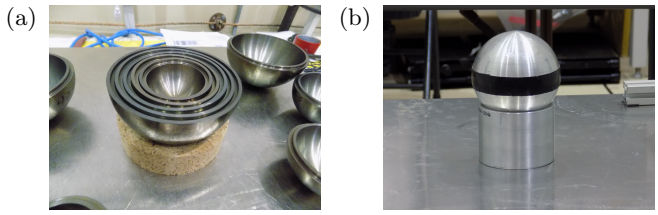

FIG. 1: (a) The interconnecting hemispheres during assembly and (b) full spherical configuration of the HEU object constructed from the Rocky Flats shells placed atop an aluminum hollow cylinder

used for fissile isotopic determination based on long-lived delayed neutron emission.

Here, we demonstrate that both the buildup and decay of long-lived β-delayed neutron emission from bulk uranium samples can be used to determine uranium enrichment. The method uses a custom-designed scintillation detector as an alternative to ^{3}He for β-delayed neutron detection and requires no calibration standards. A future development based upon these principles could result in compact, relatively inexpensive, and accurate detector-AI source system capable of isotopic measurements. Such a compact, transportable system may be attractive for a wide range of nuclear security and nonproliferation applications.

II. MATERIALS AND METHODS

The experiment was performed over a two-day period at the Device Assembly Facility (DAF), Nevada National Security Site. Measurements were performed on three different spherical metal objects: tungsten, depleted uranium (DU), and highly-enriched uranium (HEU). The object masses were 14.7 kg, 12.8 kg, and 13.8 kg, respectively. Due to constraints on the available materials and possible geometric configurations, it was not possible to use the same masses for all test objects.

The HEU object was a series of connecting concentric hemispheres of HEU known as the Rocky Flats shells, which have a bulk density of 18.664 g/cm^3 and an isotopic content of 93.16% ^{235}U, 5.35% ^{238}U, and less than 2% of other isotopes of uranium [15]. The HEU object consisted of shells labeled 01–24 and arranged in a spherical configuration, where individual shells have specific dimensions and masses stated in Ref. [15]. A photograph of the HEU object during assembly (which does not include all of the interconnecting shells) and after assembly is shown in Fig. 1.

The HEU, DU, and tungsten objects were interrogated with 14.1-MeV neutrons produced by a DT generator (Thermo Scientific model P211), with an approximate isotropic yield of 10^8 neutrons/s. Each object was placed at a distance of 13 cm, as measured from the center of the object to the neutron-generating target in the DT generator. The detector was placed on the side of the object opposite from the neutron source. The front face of the detector was located 12 cm from the center of the object. For all measurements, the DT generator was operated at a pulse rate of 100 Hz and a pulse width of approximately 10 μs.

The detector used in these measurements was a custom-built heterogeneous composite scintillator. The cylindrical detector has been constructed from enriched ^{6}Li scintillating glass and scintillating polyvinyl toluene with a height and diameter of 12.7 cm. The composite detector consists of an array of 1×1×76 mm^3 GS20 lithium glass square rods embedded in a cylinder of scintillating polyvinyl toluene (PVT) with a height and diameter of 12.7 cm. The glass rods are centered in the PVT matrix. GS20 glass is enriched to approximately 95% ^{6}Li and serves as the neutron capture material; the total lithium content in the glass is 6.6%. Fig. 2 shows a Geant4 [16] rendering of the side and top of the detector.

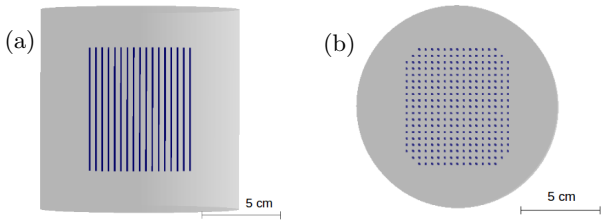

FIG. 2: Geometry of the composite neutron detector as defined in Geant4 simulation: (a) side and (b) top view

The detector was a larger version of the prototype design described in Ref. [17]. Neutrons incident onto the detector typically undergo thermalization in the PVT and are subsequently captured in the lithium-doped glass. Neutron capture on ^{6}Li has a Q-value of 4.8 MeV and produces an alpha particle and a triton. Neutron capture events can be easily distinguished from events that take place in the PVT due to unique response that results from both the Q-value of the capture reaction and different scintillation properties of PVT and glass. The intrinsic efficiency was calculated by Monte Carlo simulation for delayed neutrons from ^{235}U and ^{238}U fission, similar to method described in Ref. [9], and yielded approximately 15% for each isotope. Additionally, the detector has a simulated intrinsic efficiency of 7.8% for ^{252}Cf fission neutrons.

The detector was coupled to a Hamamatsu R6527 photomultiplier tube (PMT) and powered using a CAEN DT5533 high-voltage power supply. The output signals were collected and digitized using a CAEN DT5730 14-bit 500 MHz desktop waveform digitizer. CAEN's digital pulse processing-pulse shape discrimination (DPP-PSD) Control Software and DPP-PSD firmware were used to collect and store data for post-processing [18]. A short-gate integral (Q_{short}) and a long-gate integral (Q_{long}) were recorded for each waveform as the basis for pulse shape discrimination. The integration bounds were op-

timized prior to the experiment at t_s=34 ns for Q_{short} and t_s=150 ns for Q_{long}, where t_s is the start time of the waveform as identified by the trigger from CAEN DPP-PSD firmware. The t_s was offset by 6 ns prior to the trigger on the leading edge of the pulse.

To measure the delayed neutron time profile for each object, detector data were recorded during a series of on-off cycles of the neutron generator. In each cycle, the generator was turned on for 30 seconds, then turned off for one minute. One measurement run consisted of ten on-off cycles, lasting about 15 minutes in total. Three such measurements were taken for both the HEU and DU targets, and one was taken for tungsten. The on-off cycles were summed for final analysis. Two five-minute background measurements were also recorded, one with the HEU target in place, and the other with the DU target. Calibration measurements were performed using ^{137}Cs and AmBe sources. A photograph of the experimental setup is shown in Fig. 3.

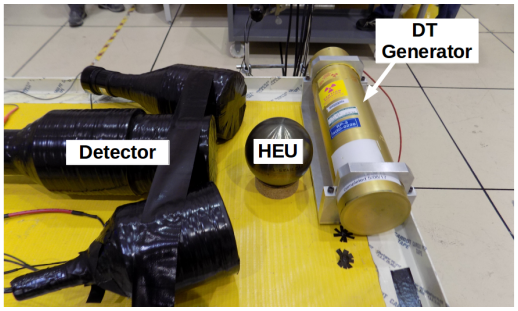

FIG. 3: Experimental setup including the composite detector coupled to the PMT, the HEU object, and the DT generator

III. RESULTS & DISCUSSION

Fig. 4 shows the PSP-light output distribution for 15 minutes of on/off cycles of the DT generator interrogating a highly enriched uranium (HEU) object. The charge integration method was used to obtain the pulse shape parameter (PSP) as follows:

$$PSP = (Q_{long} - Q_{short})/Q_{long}. \quad (1)$$

Neutron capture events are localized near PSP=0.55 and light output of approximately 0.28 MeVee. A calibration measurement using a PuBe source was used to establish a cut around the neutron capture region, where events within the cut were accepted as neutrons. A Gaussian function was fit in both dimensions to the neutron region centered at a PSP of 0.55 and light output of 0.28 MeVee in Fig. 4, and a 3σ cut used to establish the neutron capture region.

Two different long-lived β-delayed neutron signatures were measured. The first was the buildup of delayed neutron emission measured between the generator pulses;

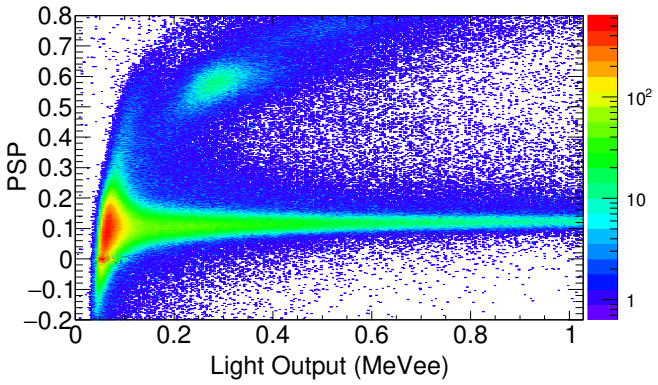

FIG. 4: PSP and light output distribution from the composite detector for the HEU object interrogated by 14.1 MeV neutrons

the second was the decay of the delayed neutron emission measured immediately after the generator had been turned off. The time profile of these two delayed neutron signatures is parameterizable in analytic form using the available nuclear data and depends on the enrichment of the uranium sample. The buildup of delayed neutron emission can be described in the framework of six delayed neutron groups by

$$R_b(t) = B + C\sum_{i=1}^{2}\sum_{j=1}^{6} f_i P_i Y_{i,j}\epsilon_{i,j}\left[1 - \exp(-t/\tau_{i,j})\right], \quad (2)$$

where $R_d(t)$ is the detected buildup of delayed neutron emission, B is the constant neutron background rate, C is a scaling constant, index i corresponds to the uranium isotope (^{235}U or ^{238}U), index j represents the delayed neutron group number, f_i is the 14-MeV neutron-induced fission probability of uranium isotope i, P_i is the isotopic percentage of uranium isotope i, $\epsilon_{i,j}$ is the detector efficiency for delayed neutron group j of uranium isotope i, $\tau_{i,j}$ is the decay constant for delayed neutron group j of uranium isotope i, and $Y_{i,j}$ is the delayed neutron yield per fission for group j of uranium isotope i. Similarly, the decay of delayed neutron emission can be expressed as

$$R_d(t) = B + C\sum_{i=1}^{2}\sum_{j=1}^{6} f_i P_i Y_{i,j}\epsilon_{i,j} \left[\exp(t_b/\tau_{i,j}) - 1\right]\exp(-t/\tau_{i,j}), \quad (3)$$

where t_b is the period over which the constant-intensity AI beam was turned on [9].

A Monte Carlo simulation was performed using Geant4 version 10.4 to estimate the intrinsic delayed neutron detection efficiency for the composite detector [16]. The energy spectra for the individual groups for ^{235}U and ^{238}U were simulated and intrinsic neutron detection efficiencies calculated on a group-by-group basis. Prior reported

TABLE I: ^{235}U delayed neutron parameters

Group	Y(%)	ϵ_C	$T_{1/2}$ (s)
1	0.063	0.163	54.5
2	0.351	0.151	21.8
3	0.310	0.150	6.00
4	0.672	0.149	2.23
5	0.211	0.149	0.496
6	0.043	0.148	0.179

TABLE II: ^{238}U delayed neutron parameters

Group	Y(%)	ϵ_C	$T_{1/2}$ (s)
1	0.054	0.163	52.4
2	0.564	0.148	21.6
3	0.667	0.153	5.00
4	1.599	0.151	1.93
5	0.927	0.151	0.490
6	0.309	0.150	0.172

energy spectra for the six delayed neutron groups of ^{235}U and ^{238}U in Ref. [19] were used in the simulation. The yields (Y), efficiencies (ϵ_C), and the half-lives ($T_{1/2}$) for the six delayed neutron groups are listed in Table I and Table II for ^{235}U and ^{238}U, respectively [20]. These efficiences were used in the parameterizations of the buildup and decay delayed neutron rate.

Eqs. (2) and (3) provide an analytical means to explore the enrichment-dependent time behavior of the two delayed neutron signatures. Fig. 5 shows the simulated buildup and decay time emission of delayed neutrons for a pure sample of ^{235}U and a pure sample of ^{238}U with $t_b = 30$ s. A qualitative inspection of Fig. 5 reveals an exploitable difference between the shapes of the two pure samples of uranium for both the delayed neutron buildup and decay time distributions.

A simple metric can be defined on the basis of the difference in the delayed neutron emission profile for ^{235}U and ^{238}U and used to quantify the enrichment. The metric is based on the ratio of the total number of detected neutrons in two separate time periods over which the delayed neutron emission is measured and may be applied to both the buildup and the decay time distribution. The metric is denoted by F and can be calculated using the following relationship:

$$F = N_1/N_2, \tag{4}$$

where N_1 and N_2 are the total number of counts within two chosen time periods, A_1 and A_2, as illustrated in an example in Fig. 6, where decay time profiles for pure samples of ^{235}U and ^{238}U immediately after the neutron generator is turned off are shown. The same methodology is applicable to the buildup of long-lived delayed neutron emission.

A measure of distinguishability, D, can be defined that takes into account the mean values of the detected neutron counts in two time periods (F) and their standard

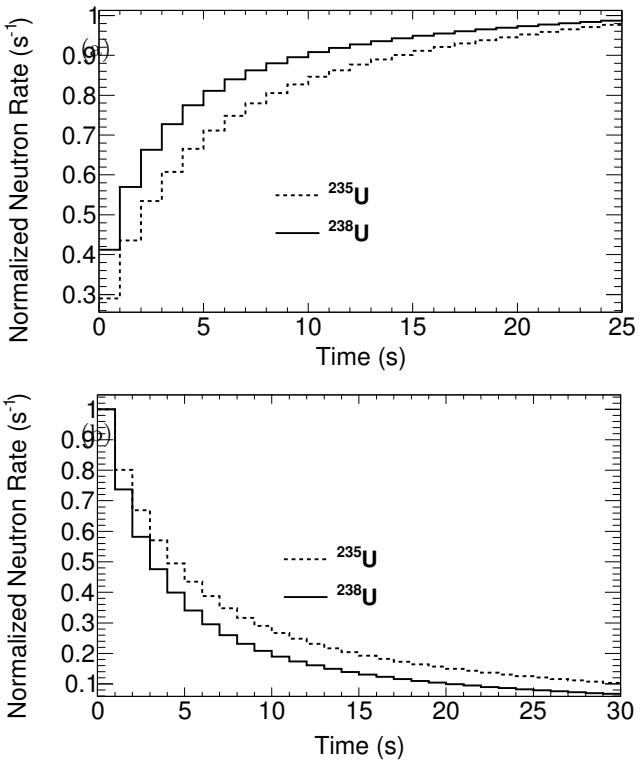

FIG. 5: Simulated long-lived (a) buildup and (b) decay of delayed neutrons for a pure ^{235}U sample and a pure ^{238}U sample

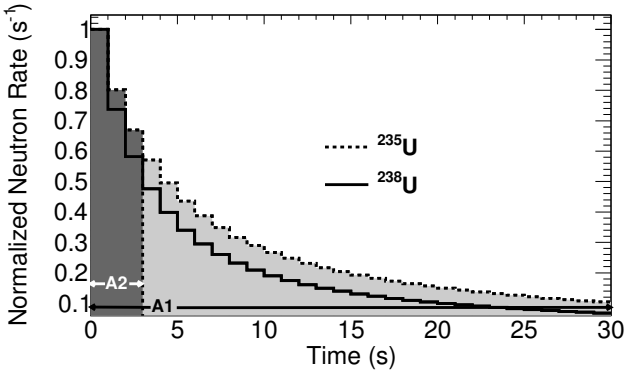

FIG. 6: The use of A_1 and A_2 limits for calculation of the ratio F. Long-lived delayed neutron decay from neutron induced fission after accelerator operation for pure samples of ^{235}U and ^{238}U is shown.

deviations (σ):

$$D = \frac{|F_{235} - F_{238}|}{\sigma_{235} + \sigma_{238}}, \tag{5}$$

where F is defined by Eq. (4) and σ is the standard deviation of F, while subscripts denote the two major isotopes of U. Since D depends not only on the characteristics of delayed neutron emission, but also on the counting statistics, the optimum start and stop times for A_1 and

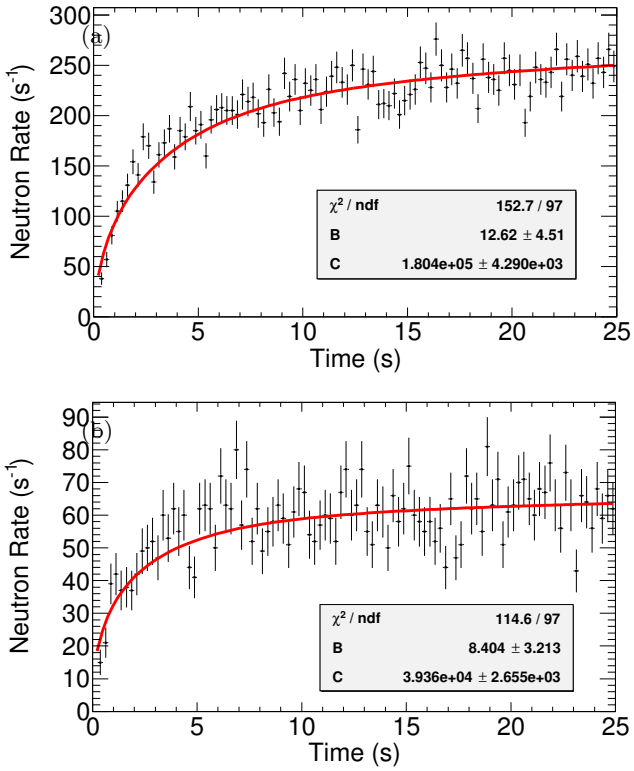

FIG. 7: Beta-delayed neutrons detected between AI pulses for (a) HEU and (b) DU when the beam is turned on ($t = 0$). The fit to model in Eq. (2) is shown in red.

A_2 depend on the number of detected neutron counts, which is affected by system efficiency and measurement time.

Fig. 7 shows the buildup of delayed neutrons between accelerator pulses for HEU and DU. The six-group delayed neutron buildup model defined in Eq. (2) is fitted to the measured buildup data for each isotope, and is shown as a red line in Fig. 7.

The period during which neutrons were produced by the DT generator was determined from the event rate recorded by the detector. The total event rate was monitored in 10-μs increments. When the total number of events in a 10-μs increment increased above twenty, the start of a new neutron generator pulse was marked. The twenty-event threshold was set empirically, based on the average number of counts observed in 10-μs increments when the generator was operating. The 10-μs increment was chosen to match the pulse duration of the generator.

To allow for neutron die-away, events occurring withing 4.5 ms following a generator pulse were disregarded. The neutron events occurring in the remaining 5.5 ms preceding the next generator pulse were used to measure the delayed neutron buildup. Fig. 8 shows the summed neutron rate for approximately fifteen minutes of generator operation with a HEU test object. The neutron die-away is apparent in the approximate period of 0–4.5 ms. Fig. 9

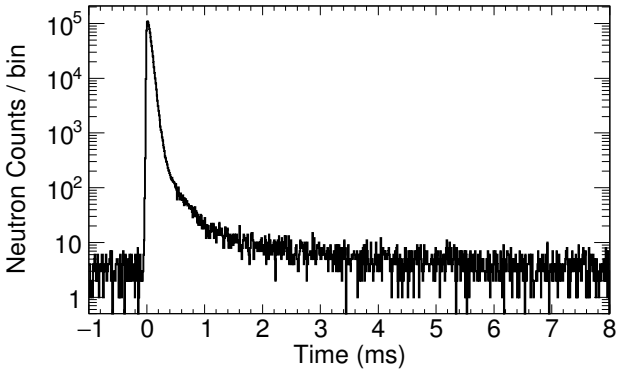

FIG. 8: Summed neutron rate determined from approximately 15 minutes of DT generator operation

illustrates the period between generator pulses within which neutron events were selected to measure the delayed neutron buildup and the prompt die-away region, where events were rejected.

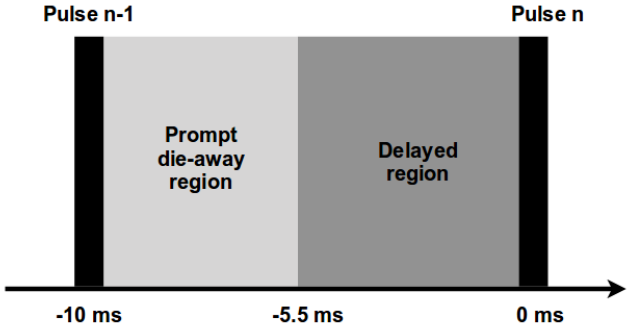

FIG. 9: Graphical representation of the prompt die-away and delayed region for neutron event selection

Fig. 10 shows the decay of delayed neutrons after the accelerator is turned off for HEU and DU. The six-group delayed neutron decay model defined in Eq. (3) is fitted to the measured decay data for each isotope, and similarly shown in Fig. 10. Higher delayed neutron count rates are observed for HEU in both the buildup and decay time distributions. This is expected due to the greater HEU object mass and higher delayed neutron microscopic fission cross-section of the HEU sample for 14.1 MeV neutrons.

In addition to HEU and DU objects, a tungsten object was also measured. The neutron buildup and decay rates were measured in the same manner as for the uranium objects and are shown in Fig. 11. There was no appreciable neutron rate observed in either the buildup or decay time periods.

An optimization of D was performed for the measured delayed neutron buildup and decay rates. The start and stop times for A_1 were fixed to 0 and 25 s for the buildup

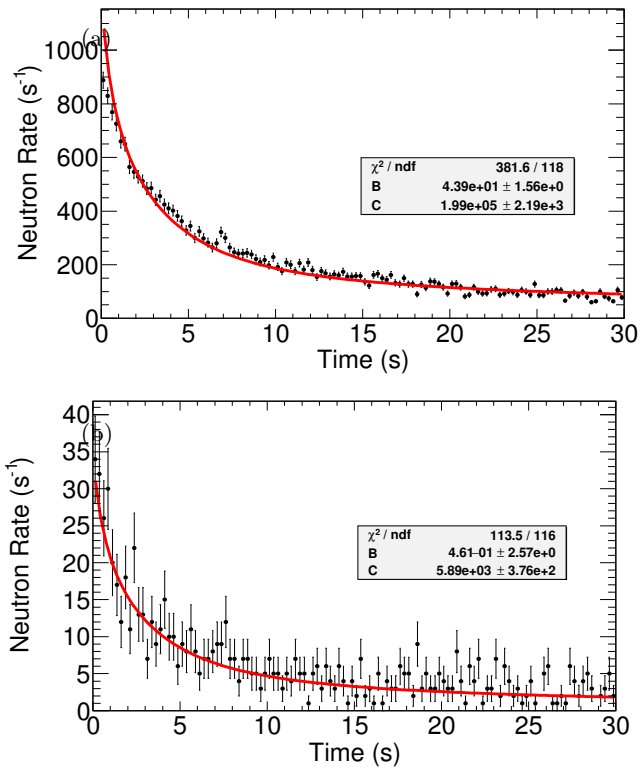

FIG. 10: Beta-delayed neutrons observed after AI beam is turned off ($t_b = 30$ s) for (a) HEU and (b) DU. The fit to model in Eq. (3) is shown in red.

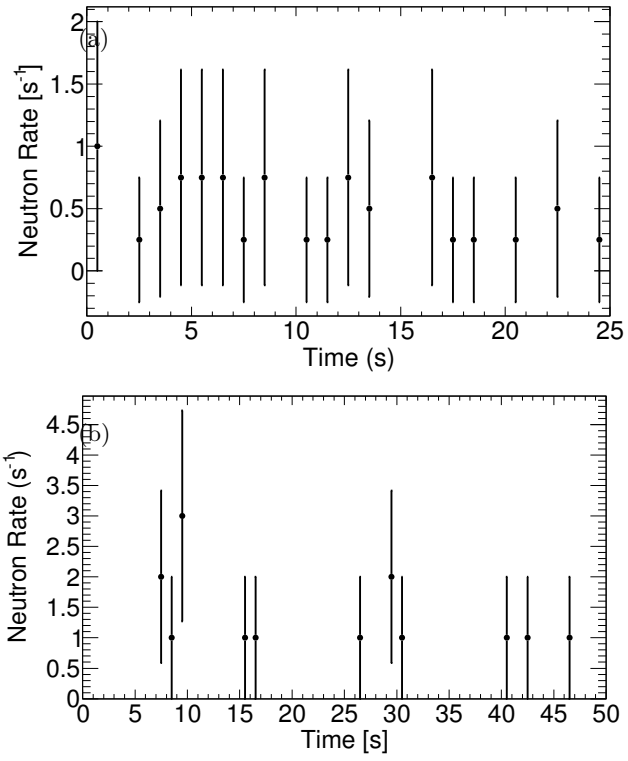

FIG. 11: Detected neutron rate observed (a) between AI pulses, with the generator turned on ($t = 0$) and (b) after the generator has been turned off ($t = 0$) for the tungsten object

time distribution and 0 and 30 s for the decay time distribution. The value of D for all combinations of the start and stop times of A_2 was then calculated. Fig. 12 shows a 2D histogram of different start and stop times for A2 and the resulting D for the buildup of delayed neutrons. The maximum value of D in Fig. 12 represents the greatest degree of differentiability between ^{235}U and ^{238}U. A start time of 0 s and a stop time of 4 s corresponding to the maximum value of D was selected for A_2 for the buildup of delayed neutrons. Similarly, an optimization of D for the decay of delayed neutrons was performed, resulting in an A_2 start time of 0 s and stop time of 3 s.

The F values for the buildup and decay are unique for a given enrichment. Using the optimized limits of A_2 for both the buildup and decay of delayed neutrons, experimental F values were calculated for the HEU and DU samples. The experimental results are shown in Fig. 13 along with the simulated F values for the buildup and decay of delayed neutrons for enrichment levels ranging from 0 to 100%.

The F values calculated from the experimental results can be used to establish a range of enrichment for the interrogated object. Table III shows the calculated range of enrichment based on the measurement. The uncertainty in the calculated enrichment is smaller for the HEU sample due to its higher neutron rates. Even with

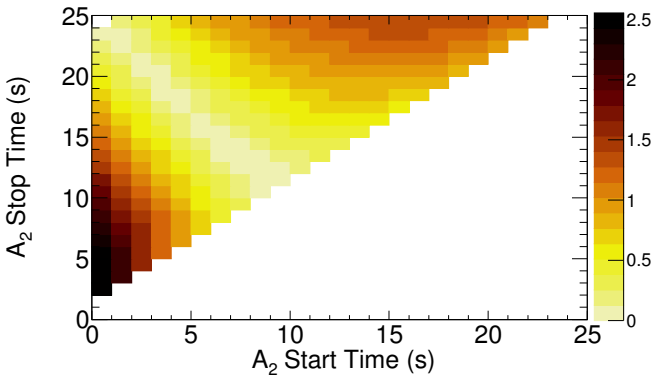

FIG. 12: Optimization of D based on varying start and stop times of area A_2 for the buildup of delayed neutrons

the relatively low statistics available in this experiment in which the detector subtended only a small solid angle, important conclusions can be quickly drawn about the interrogated objects. First, the presence of HEU can be confirmed by measuring either the buildup or the decay neutron emission rate. The enrichment of the DU object had an upper bound of 25%, which is well below weapons-grade HEU levels. Finally, the control tungsten

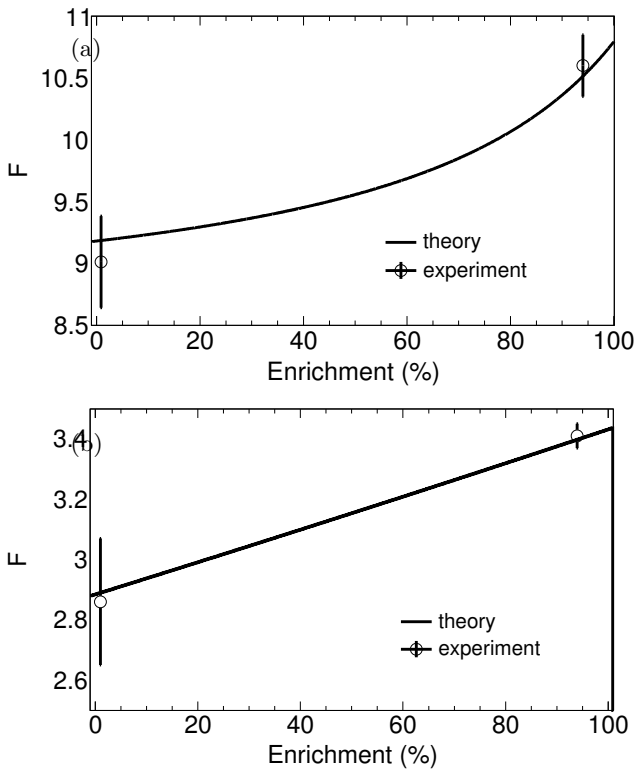

FIG. 13: Simulated and measured F values for the (a) buildup and (b) decay of delayed neutrons for varying levels of enrichment

TABLE III: Uranium enrichment 1σ range inferred from the experiment and comparison with the actual enrichment

Sample	Actual	Buildup	Decay	Combined
HEU	93.2%	$92.7^{+7.3}_{-3.3}$%	100^{+0}_{-14}%	$96.3^{+3.7}_{-7.1}$%
DU	0.7%	0^{+35}_{-0}%	7^{+28}_{-7}%	$3.5^{+21.3}_{-3.5}$%

object was confirmed not to contain appreciable quantity of fissionable material. Accuracy of these measurements could be greatly improved with longer counting times and larger detector coverage area.

In conclusion, we demonstrated a method that can be used to determine uranium enrichment using both the delayed neutron buildup or the decay time emission profile. The shape of the delayed neutron time profile, and thus the enrichment metric used, are not expected to be sensitive to shielding and self-shielding, as is the case with the alternative method that employs the intensities of characteristic γ rays. With greater detector coverage and longer counting times, this technique could prove to be a powerful tool for uranium enrichment determination in various nonproliferation applications. By employing capture-gated composite scintillation detectors similar to the one employed in this proof-of-concept study, large coverage could be realized at a cost that is low to moderate and employs no ^{3}He detectors. Measuring enrichment values over the full range of enrichment would further validate the performance of this technique, which is one of the future experimental goals.

ACKNOWLEDGMENTS

The authors would like to thank J. Mattingly of North Carolina State University and J. Hutchinson of Los Alamos National Laboratory for assistance with planning and carrying out the experiment, and K. Wilhelm, F. Sutanto, and M. Sharma for their assistance with modeling. This work was partially supported by the U.S. Department of Homeland Security (2014-DN-077-ARI078-02 and 2015-DN-077-ARI096) and by the Consortium for Verification Technology under U.S. Department of Energy National Nuclear Security Administration award number DE-NA0002534. The research of J.N. was performed under appointment to the Nuclear Nonproliferation International Safeguards Fellowship Program sponsored by the National Nuclear Security Administration's Office of International Safeguards (NA-241).

[1] R. Berndt, E. Franke, and P. Mortreau, ^{235}U enrichment or UF_6 mass determination on UF_6 cylinders with non-destructive analysis methods, Nucl. Instrum. Methods Phys. Res., Sect. A **612**, 309 (2010).

[2] R. Runkle, A. Bernstein, and P. Vanier, Securing special nuclear material: Recent advances in neutron detection and their role in nonproliferation, J. Appl. Phys. **108**, 111101 (2010).

[3] T. Reilly, R. Walton, and J. Parker, Progress report LA-4605-MS, Los Alamos National Laboratory, NNM (197) **19** (1970).

[4] R. Augustson and T. Reilly, Fundamentals of passive nondestructive assay of fissionable material, AEC Contract W-740 S-ENG. 36 , 1 (1974).

[5] P. Matussek, Accurate determination of the ^{235}U isotope abundance by gamma spectrometry, Tech. Rep. KFK–3752 Kernforschungszentrum Karlsruhe G.m.b.H. (1985).

[6] N. Bohr and J. A. Wheeler, The mechanism of nuclear fission, Phys. Rev. **56**, 426 (1939).

[7] M. Kinlaw and A. Hunt, Fissionable isotope identification using the time dependence of delayed neutron emission, Nucl. Instrum. Methods Phys. Res., Sect. A **562**, 1081 (2006).

[8] P. Rose, A. Erickson, M. Mayer, J. Nattress, and I. Jovanovic, Uncovering special nuclear materials by low-

energy nuclear reaction imaging, Sci. Rep. **6** (2016).
[9] M. Mayer, J. Nattress, and I. Jovanovic, Detection of special nuclear material from delayed neutron emission induced by a dual-particle monoenergetic source, Appl. Phys. Lett. **108**, 264102 (2016).
[10] C. Moss, M. Brener, C. Hollas, and W. Myers, Portable active interrogation system, Nucl. Instrum. Methods Phys. Res., Sect. B **241**, 793 (2005).
[11] R. Runkle, D. Chichester, and S. Thompson, Rattling nucleons: New developments in active interrogation of special nuclear material, Nucl. Instrum. Methods Phys. Res., Sect. A **663**, 75 (2012).
[12] W. Myers, C. Goulding, and C. Hollas, Determination of the ^{235}U enrichment of bulk uranium samples using delayed neutrons, Tech. Rep. No. LA-UR-06-3984, Los Alamos National Laboratory (2006).
[13] M. Sellers, D. Kelly, and E. Corcoran, An automated delayed neutron counting system for mass determinations of special nuclear materials, J. Radioanal. Nucl. Chem. **291**, 281 (2012).
[14] X. Li, R. Henkelmann, and F. Baumgrtner, Rapid determination of uranium and plutonium content in mixtures through measurement of the intensity time curve of delayed neutrons, Nucl. Instrum. Methods Phys. Res., Sect. B **215**, 246 (2004).
[15] R. Rothe, Extrapolated experimental critical parameters of unreflected and steel-reflected massive enriched uranium metal spherical and hemispherical assemblies, Tech. Rep INEEL/EXT-97-01401, Lockheed Idaho Technologies Co., Idaho National Engineering and Environmental Lab. (1997).
[16] S. Agostinelli *et al.*, Geant4–simulation toolkit, Nucl. Instrum. Methods Phys. Res., Sect. A **506**, 250 (2003).
[17] M. Mayer, J. Nattress, V. Kukharev, A. Foster, A. Meddeb, C. Trivelpiece, Z. Ounaies, and I. Jovanovic, Development and characterization of a neutron detector based on a lithium glasspolymer composite, Nucl. Instrum. Methods Phys. Res., Sect. A **785**, 117 (2015).
[18] DPP-PSD User Manual - UM2580, (2015), User's Manual for the DT 5730.
[19] D. Saphier, D. Ilberg, S. Shalev, and S. Yiftah, Evaluated delayed neutron spectra and their importance in reactor calculations, Nucl. Sci. and Engineering **62**, 660 (1977).
[20] G. R. Keepin, T. Wimett, and R. Zeigler, Delayed neutrons from fissionable isotopes of uranium, plutonium and thorium, J. Nucl. Energy **6**, IN2 (1957).